optical trap, which is readily available in many laboratories.

A combination of the gates $U_1^{(j)}$ and $U_2^{(j)}$ permits us to implement any single-bit operation, which together with the nontrivial two-bit gate $U_3^{(jk)}$ between the qubits j,k are enough for universal quantum computation. To construct the gate $U_3^{(jk)}$ using geometric means, we need to exploit the Coulomb interactions between the ions. For this purpose, we provide a scheme based on a recent dynamical proposal (*14*), which uses two-color laser manipulation. The transition $|1\rangle \rightarrow |e\rangle$ for the j,k ions is driven by a red and a blue detuned laser, respectively, with detunings $-(\nu + \delta)$ and $\nu + \delta$ (Fig. 2), where ν is the phonon frequency of one oscillation mode (normally the center of mass mode) and δ is an additional detuning. Similarly, the transition $|a\rangle \rightarrow |e\rangle$ is also driven by a red and a blue detuned laser, but with the additional detuning $\delta' \neq \delta$ to avoid the direct Raman transition. For simplicity, here we choose $\delta' = -\delta$ as in Fig. 2. Under the condition of strong confinement $\eta^2 \ll 1$ (the Lamb-Dicke criterion), where η is defined by the ratio of the ion oscillation amplitude to the manipulation optical wave length, the Hamiltonian describing the interaction has the form

$$H_{jk} = \frac{\eta^2}{\delta}[-|\Omega_1|^2\sigma_{j1}^{\varphi_1}\sigma_{k1}^{\varphi_1} + |\Omega_a|^2\sigma_{ja}^{\varphi_a}\sigma_{ka}^{\varphi_a}], \tag{2}$$

where $\sigma_{j\mu}^{\varphi_\mu} \equiv e^{i\varphi_\mu}|e\rangle_j\langle\mu| + \text{h.c.}$ ($\mu = 1,a$) and Ω_1, Ω_a are the corresponding Rabi frequencies, respectively, with the phases φ_1, φ_a. In writing the Hamiltonian (Eq. 2), we have neglected some trivial light shift terms that can be easily compensated, for instance, by another laser. To get a geometric operation, we choose the relative intensity $|\Omega_1|^2/|\Omega_a|^2 = \tan(\theta/2)$ and phase $\varphi_1 - \varphi_a = \varphi/2$, with the control parameters θ,φ undergoing a cyclic adiabatic evolution from $\theta = 0$. During the evolution, the computational bases $|00\rangle_{jk}$, $|01\rangle_{jk}$, and $|10\rangle_{jk}$ are decoupled from the Hamiltonian (Eq. 2), while the $|11\rangle_{jk}$ component adiabatically follows as $\cos\frac{\theta}{2}|11\rangle_{jk} + \sin\frac{\theta}{2} e^{i\varphi}|aa\rangle_{jk}$, which acquires a Berry phase after the whole loop. So we get the conditional phase-shift gate $U_3^{(jk)}$ with the purely geometric phase $\phi_3 = \oint d\Omega$, the swept solid angle by the vector (θ,φ). This geometric two-bit gate has shared the advantages of the recently proposed and demonstrated dynamical scheme (*14*, *18*) in the sense that, first, the ion motional modes need not be cooled to their ground states as long as the Lamb-Dicke criterion is satisfied; and second, separate addressing of the ions is not needed during the two-bit gate operation.

For experimental demonstration of the above universal set of geometric gates, we need to consider several kinds of decoherence that impose concrete conditions on the relevant parameters. First, one should fulfill the adiabatic condition. This means the gate operation time should be larger than the inverse of the energy gap between the dark states and the bright and excited states. The energy gap is given by $\Delta_1 = |\Omega|$ for the single-bit gates and by $\Delta_2 = \eta^2|\Omega|^2/\delta$ for the two-bit gate. So we require that the single-bit and two-bit gate operation times t_i^g ($i = 1, 2$) be reasonably long, so that the leakage error to the bright and the excited states, which scales as $1/(\Delta_i t_i^g)^2$, is small. Second, we need to avoid spontaneous emission (with a rate γ_s) of the excited state $|e\rangle$. Because of the adiabatic condition, the excited state is only weakly populated even though we use resonant laser coupling, and the effective spontaneous emission rate is reduced by the leakage probability $1/(\Delta_i t_i^g)^2$. As a result, we only require $\gamma_s/(\Delta_i^2 t_i^g) \ll 1$ for the spontaneous emission to be negligible during the gate operation. Finally, the influence of the heating of the ion motion should be small. We assume that all the manipulation lasers are copropagating, so that the heating caused by the two-photon recoils is negligible. The carrier phononic states are only virtually excited during the two-bit gate, so the influence of the heating rate γ_h is reduced by the phonon population probability $\eta^2|\Omega|^2/\delta^2$. The effective heating rate should be much smaller than the gate speed, which requires $\delta \gg \gamma_h$. All the conditions discussed above in the geometric gates are exactly parallel to those in the dynamical schemes using the off resonant Raman transitions. The reason for this is that, in both cases, the excited state is only weakly populated and the population probability obeys the same scaling law, although the physical mechanism for the weak population is quite different. So, compared with the dynamical schemes, our requirements are not more stringent. However, the geometric proposal introduced in this paper will permit us to experimentally investigate the fundamental Abelian and non-Abelian holonomies (*10*) and may open new possibilities for robust quantum computation (*21*, *22*).

References and Notes

1. D. P. DiVincenzo, *Science* **270**, 255 (1995).
2. J. A. Jones, V. Vedral, A. Ekert, G. Castagnoli, *Nature* **403**, 869 (1999).
3. G. Falci *et al.*, *Nature* **407**, 355 (2000).
4. P. Zanardi, M. Rasetti, *Phys. Lett. A* **264**, 94 (1999).
5. J. Pachos, P. Zanardi, M. Rasetti, *Phys. Rev. A* **61**, 010305(R) (2000).
6. J. Pachos, Lawrence Berkeley National Laboratory (LANL) preprint available at http://xxx.lanl.gov/abs/quant-ph/0003150.
7. J. Pachos, P. Zanardi, LANL preprint available at http://xxx.lanl.gov/abs/quant-ph/0007110.
8. M. V. Berry, *Proc. R. Soc. London A* **392**, 45 (1984).
9. F. Wilczek, A. Zee, *Phys. Rev. Lett.* **52**, 2111 (1984).
10. A. Shapere, F. Wilczek, *Geometric Phases in Physics* (World Scientific, Singapore, 1989).
11. S. Lloyd, *Phys. Rev. Lett.* **75**, 346 (1995).
12. J. I. Cirac, P. Zoller, *Phys. Rev. Lett.* **74**, 4091 (1995).
13. A. Sorensen, K. Molmer, *Phys. Rev. Lett.* **82**, 1971 (1999).
14. K. Molmer, A. Sorensen, *Phys. Rev. Lett.* **82**, 1835 (1999).
15. J. I. Cirac, P. Zoller, *Nature* **404**, 579 (2000).
16. C. Monroe *et al.*, *Phys. Rev. Lett.* **75**, 4714 (1995).
17. Ch. Roos *et al.*, *Phys. Rev. Lett.* **83**, 4713 (1999).
18. C. A. Sackett *et al.*, *Nature* **256**, 256 (2000).
19. J. Pachos, S. Chountasis, *Phys. Rev. A* **62**, 052318-1 (2000).
20. P. G. Kwiat, R. Y. Chiao, *Phys. Rev. Lett.* **66**, 588 (1991).
21. A. Y. Kitaev, LANL preprint available at http://xxx.lanl.gov/abs/quant-ph/9707021.
22. J. Preskill, LANL preprint available at http://xxx.lanl.gov/abs/quant-ph/9712048.

23. We thank P. Zanardi and J. Pachos for helpful discussions. Supported by the Austrian Science Foundation, the Europe Union project EQUIP, the European Science Foundation, the European TMR network Quantum Information, and the Institute for Quantum Information.

8 January 2001; accepted 11 April 2001

Explaining the Weddell Polynya—a Large Ocean Eddy Shed at Maud Rise

D. M. Holland

Satellite observations have shown the occasional occurrence of a large opening in the sea-ice cover of the Weddell Sea, Antarctica, a phenomenon known as the Weddell Polynya. The transient appearance, position, size, and shape of the polynya is explained here by a mechanism by which modest variations in the large-scale oceanic flow past the Maud Rise seamount cause a horizontal cyclonic eddy to be shed from its northeast flank. The shed eddy transmits a divergent Ekman stress into the sea ice, leading to a crescent-shaped opening in the pack. Atmospheric thermodynamical interaction further enhances the opening by inducing oceanic convection. A sea-ice–ocean computer model simulation vividly demonstrates how this mechanism fully accounts for the characteristics that mark Weddell Polynya events.

The Weddell Polynya—the largest observed sea-ice anomaly of the polar oceans—is a hole in the sea-ice cover of the Weddell Sea, Antarctica, that can occupy an area of well over 200,000 km^2, a size comparable to the island of Great Britain. The appearance of this polynya (*1*) is irregular in its timing, location, and shape. An explanation for the cause of this phenomenon has remained elusive, but the presence of a nearby massive seamount, Maud Rise, has long been suspected as playing a key role. This report explains the occurrence of the Weddell Polynya via a mechanism that is fundamentally dynamical in origin and not thermodynamical, as is often supposed (*2*).

Most of our knowledge of the cryosphere in this region comes from satellite data collected over almost three decades. During 1974–76, the Weddell Polynya was at its largest extent ever observed (~200,000 km^2). That event was remarkable because after its initial appearance in the winter of 1974 (and despite the fact that the sea-ice cover in the region is completely removed during summer by solar radiation), the polynya reappeared in two subsequent winters. During its initial appearance, in July of 1974, the polynya occupied its most northeastern position, extending over the northeast flank of Maud Rise, along the east and south flanks of the seamount, and to the area to the west-southwest, away from the seamount. There was, by contrast, near complete sea-ice coverage along the west and north flanks of the seamount. At its mid-life, in winter of 1975, it was not the northeast flank but the east and south flanks that remained sea-ice free (Fig. 1A). In its third and final year, the polynya drifted sufficiently west-southwestward such that no sea-ice–free area was found in the vicinity of Maud Rise. Since that event of the mid-1970s, the sea-ice cover in the Weddell Sea has remained rather complete in its areal coverage, including over the Maud Rise region, with occasional anomalies appearing on the satellite-derived sea-ice concentration maps, indicating a partial opening in the sea-ice cover.

Our knowledge of the hydrography in this region has been substantially enhanced by a dedicated oceanographic field campaign undertaken during the austral winter of 1994 (*3*). An analysis of the data collected shows that, at least at the time of the measurements, there existed a halo feature (*4*), elliptical in shape of about 60 km by 150 km in lateral dimensions, located along the southwest flank of Maud Rise and containing a pool of water with an elevated thermocline and anticyclonic vorticity. Farther to the west-southwest, away from the seamount, was another pool of warm water, having noticeably cyclonic vorticity. Coincidentally, during the field campaign, a crescent-shaped polynya appeared over the northeast flank of the seamount (Fig. 1B). This simultaneous observation of a halo-shaped region with an elevated thermocline on the southwest flank of the seamount and a polynya appearing on the northeast flank is an important point later referenced.

Explanations for the occurrence of the Weddell Polynya are varied, ranging from considerations of the modifications of the lower atmospheric wind field (*5–7*), to ocean surface preconditioning (*8, 9*), to Taylor cap formation (*10, 11*). Previous studies, however, do not confidently explain the mechanism that leads to polynya formation. This motivates the development of a theory to be constructed by combining relevant knowledge about ocean and sea-ice dynamics in a novel way. This was done in the unique bathymetric context of the eastern Weddell Sea, where the Maud Rise seamount reaches from the relatively flat surrounding abyssal plain at a depth of greater than 5000 m upward toward the surface, reaching to within less than 2000 m of that surface (Fig. 2).

The starting point for relevant ocean dynamics is establishing how ocean waters behave when they encounter a seamount (*12*). A temporally varying ocean current interacting with a seamount redistributes fluid in such a way that waters with anticyclonic vorticity and elevated isopycnals exist over the right flank (looking in the downstream direction) as well as over the seamount proper. Waters shed from above the seamount sink along the left flank (looking in the downstream direction) and generate cyclonic vorticity and depressed isopycnals. For sufficiently strong oncoming flows, the shed fluid continually drifts downstream in the form of a cyclonic eddy. For weaker flows, the cyclonic eddy may remain trapped in the vicinity of the seamount. Subsequent studies have verified the generality of these results, particularly for low Rossby number flows (*13, 14*).

Moving from the generality of oceanic flow past a seamount to the specific context of the Maud Rise environment, one can use knowledge of the observed flow past the seamount (*15*). An analysis of climatological hydrographic data (*16*) indicates that a flow toward the southeast is the geostrophically favored flow direction for waters impinging on the seamount. There is likely substantial fluctuation in the flow approach direction as well as in strength. Taking this southeastward flow as representative of the climatological flow toward Maud Rise, it follows as a dynamical consequence that fluctuations in the strength of that flow will lead to a large

Center for Atmosphere-Ocean Science, Courant Institute of Mathematical Sciences and Faculty of Arts and Science, New York University, New York, NY 10012, USA. E-mail: holland@cims.nyu.edu

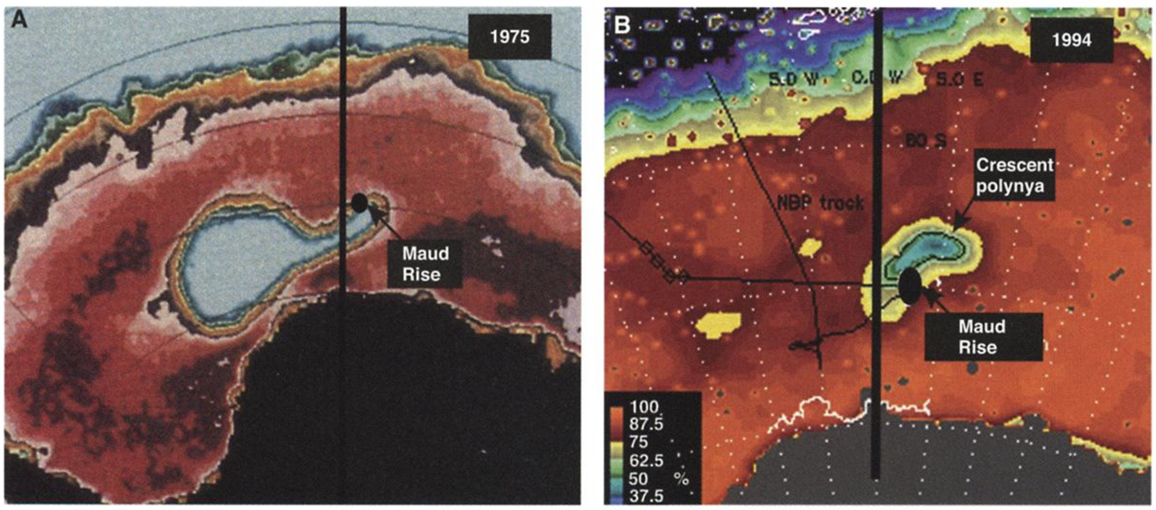

Fig. 1. (**A**) Passive-microwave satellite image showing sea-ice concentration during September 1975 (*27*). The red and brown shadings represent near complete sea-ice coverage, and the light blue represents effectively no cover. Maud Rise is shown as the black oval near the center of the image, and the thick vertical black line is the Greenwich meridian. (**B**) Passive-microwave satellite image showing sea-ice concentration during August 1994 (*28*). The sea-ice concentration is given by the color bar, with orange representing nearly complete coverage and green to blue showing the polynya as concentrations at or below 50%. Maud Rise is shown as the black oval near the center of the image and the thick vertical black line is the Greenwich meridian. The newly formed polynya assumes a crescent shape and appears over the northeast flank of the seamount.

anticyclonic eddy, with upward domed isopycnals, attaching on the southwest flank and a large cyclonic eddy, with downward domed isopycnals, shedding on the northeast flank (*12, 17*). Once shed, the cyclonic eddy will be advected southward, along the east flank of the seamount, then westward around the south flank. At that juncture, the cyclonic eddy will separate away from the proximity of Maud Rise and travel west-southwestward along with the mean background flow of the Weddell Gyre (*15*).

This is a distinct view of the circulation in the eastern Weddell Sea in that it gives special attention to the transient aspects of the environmental flow, both direction and strength, and less to the mean state, which is not fully understood. This report argues that the transient nature and appearance of the Weddell Polynya are due entirely to the transient nature of the flow impinging on Maud Rise and the aperiodic shedding of a large cyclonic eddy off the northeast flank of the seamount. This is the first half of a theory of polynya formation.

The second half of this theory draws on a basic fact of sea-ice dynamics known for almost a century (*18, 19*). The stress induced in the sea-ice cover by an underlying ocean current causes the sea ice to flow to the left of the ocean current direction by $\sim 20°$, at least for sea-ice thickness typical of the eastern Weddell Sea. Though it can be shown by a more formal analysis (*20*), simply stated, an anticyclonic ocean eddy imparts a convergent strain into the sea-ice flow, whereas a cyclonic ocean eddy imparts a divergent strain.

I now join the two theoretical constructs and present their logical implications. In the Maud Rise region, the anticyclonic vorticity that forms on the southwest flank will there impart a convergent strain into the sea ice. Despite the fact that locally raised isotherms are associated with this anticyclonic vorticity, hence possibly favoring this region for convective overturning, it is the convergent sea-ice strain, brought on by the anticyclonic vorticity, that tightens the sea-ice pack and reduces the amount of open water accessible to the atmosphere through leads. The waters over the seamount proper are also dominated by anticyclonic vorticity; hence, the same argument applies there. So, despite the thermocline shoaling over the southwest flank and over the seamount proper, the convergent strain transmitted into the sea-ice cover closes off the lead fraction and thus blocks the atmosphere from gaining access to the ocean surface in these areas. The occurrence of open-ocean convection is then not possible.

The implications for a cyclonic eddy, shed from the northeast flank, are the opposite. As a consequence of water columns being stretched while flowing off the seamount, the thermocline in the cyclonic eddy will be locally depressed. The cyclonic vorticity in the eddy transmits a divergent strain to the sea ice that enhances the open-water fraction. The sea ice moves away from the center of the cyclonic eddy, the atmosphere gains unfettered access to the ocean surface, and open-ocean convection ensues. Ironically, it is the waters in the cyclonic eddy, with their initially depressed thermocline, that are actually ventilated by vertical convective processes, and not those in the anticyclonic eddies, which had their thermocline raised. This theory predicts that a polynya will first appear along the northeast flank of Maud Rise and will subsequently advect southward along the east flank of Maud Rise, following with the mean background flow.

To test this dynamical mechanism, I configured a coupled sea-ice ocean general circulation model (*21, 22*) in a domain that represents an idealization of Maud Rise and the surrounding abyssal plain. The model geometry represents Maud Rise (Fig. 2) by interpolating the observed bathymetric data (*23*) to fit a Gaussian-profile seamount rising to within 2000 m of the sea surface, originating from a flat abyssal plain of 5000-m depth. The domain is configured as a channel such that the right and left opposite sidewalls are set as reentrant boundaries, normal to the principal direction of the imposed background flow past the seamount, whereas the two opposite sidewalls are set as solid boundaries. The model is integrated for a 30-day simulation period, starting with an imposed uniform flow of 10 cm/s. The direction of the imposed flow toward the seamount is from left to right in the computer simulations as the reentrant channel is aligned in that sense. The fluid in the channel has horizontally uniform properties and is vertically assigned properties representing an idealization of the observed hydrographic data (*16*). An initially horizontally uniform sea-ice pack of 100% concentration and 1.0-m thickness covers the entire surface of the model ocean. A horizontally uniform upward atmospheric heat flux, corresponding to a sea-ice growth rate of 3 cm/day, is imposed. Through a mixed-layer turbulence scheme (*24*), this buoyancy loss can generate vertical convection that may further enhance any transient opening by bringing up warm deep waters.

In discussing the model simulations, I translate the model orientation to the real Maud Rise region. Looking in the downstream direction of the imposed flow, the model right flank corresponds to the Maud Rise southwest flank and the model left flank corresponds to the Maud Rise northeast flank (*25*).

Ocean fluid that approaches the model seamount undergoes vortex squashing as it encounters the shoaling topography. The fluid acquires anticyclonic vorticity and moves around to the right flank of the seamount, looking in the downstream direction. Locally, the isopycnals are raised, implying that the warm deep water is brought closer to the surface. On the right flank of the seamount, the oceanic flow streamlines are dominated by anticyclonic circulation (Fig. 3A). This region of anticyclonic vorticity and domed isopycnals corresponds to the "halo" region seen in the hydrographic observations along the southwest flank of the seamount (*4*). The model sea-ice cover over the right flank (and over the seamount itself) thus experiences a convergent strain due to the anticyclonic ocean flow. Despite the model isopycnals being domed upward over the right flank and the implication of a possibly large oceanic vertical heat flux, this is not a region of polynya formation. In the context of the Maud Rise region, this model result corresponds to the southwest flank, historically a region where the initiation or appearance of a polynya has not been detected.

The left flank of the model seamount,

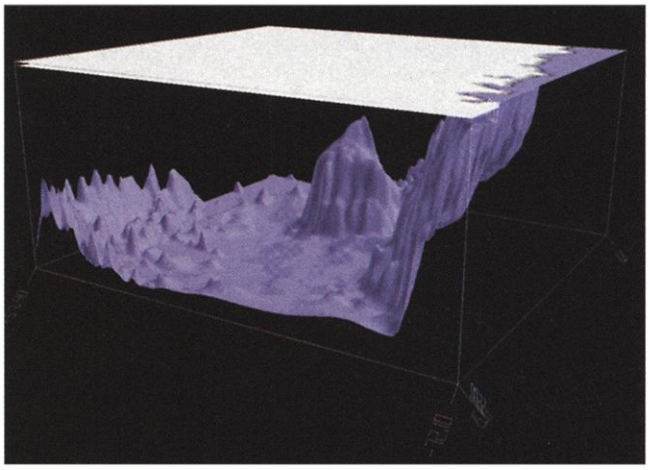

Fig. 2. Perspective view from the southwest of the sea-floor bathymetry (blue shading) in the eastern Weddell Sea (*23*). The dominant feature is the massive Maud Rise seamount (near the center of the image). To the south (right side of image), the bathymetry rises to meet the Antarctic coastline. A white horizontal surface is placed at sea level as a reference plane for the location of the sea-ice cover.

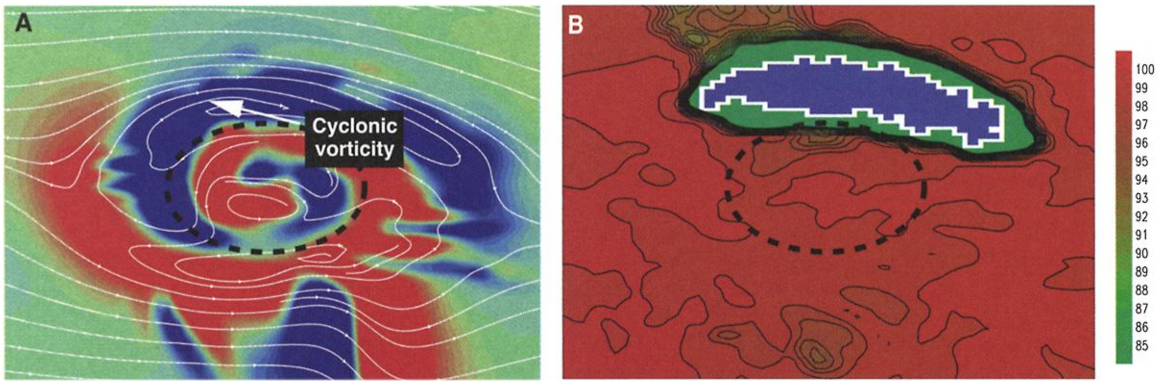

Fig. 3. (**A**) Plan view of an approximately 500 km by 500 km box showing the state of the model ocean surface flow after 30 days of simulation. The box is a truncation of a larger 1000 km by 1000 km computational domain. The black dashed oval indicates the position of the underlying idealized seamount. The white streamlines indicate the flow directions of the ocean surface waters. The color shading underlying the streamlines indicates the sense of vorticity of the flow, with green shading for regions of no vorticity, red for anticyclonic vorticity, and blue for cyclonic vorticity. The imposed mean flow direction is left to right. Looking downstream, the left flank of the seamount has an eddy that reveals an intense patch of cyclonic vorticity (blue shading). (**B**) The model sea-ice concentration field reveals a huge crescent-shaped polynya that has opened on the left flank, looking in the downstream flow direction, of the seamount. The concentration percentages are given by the color bar. The complete absence of sea ice is marked by the blue shading, which represents the open-ocean surface. The polynya has been opened by the divergent Ekman stresses associated with a cyclonic ocean eddy lying beneath. Subsequent ocean vertical convective processes in the polynya region have penetrated to a depth of almost 1 km.

looking in the downstream direction, tells a different story. As fluid columns move off the seamount, being displaced by those moving onto the seamount from the right flank, the fluid columns undergo vortex stretching and acquire cyclonic vorticity. A relatively intense patch of cyclonic vorticity is seen in the model ocean flow streamlines along the left flank (Fig. 3A). A huge crescent-shaped polynya opens in the sea-ice cover (Fig. 3B) on the left flank of the seamount because of divergent strain brought on by the oceanic cyclonic vorticity. The feature has dimensions of approximately 250 km by 100 km. The size and the approximate length-to-width ratio of 2 to 1 of the modeled polynya is consistent with the size and aspect ratio of the transient polynya observed northeast of Maud Rise, for example, during 1994 (Fig. 1B).

This interaction between a transient in the ambient ocean flow, a seamount, a shed cyclonic eddy, and a divergent Ekman stress in the sea-ice cover explains the transient polynyas that have appeared along the flanks of Maud Rise, as seen in satellite data over the past decades. It is almost certainly the mechanism by which the spectacular polynya of the 1970s was triggered (Fig. 1A). In winter 1973, the year before the onset of that major event, the sea-ice cover was unambiguously identified as being weakest in the area east of Maud Rise (*26*), a region argued here as prone to containing a cyclonic eddy shed from Maud Rise. Subsequent atmospheric processes, as well as a less stratified ocean (thus more favorable to convection), likely favored that event as ultimately becoming the biggest polynya yet seen—a kind of "super polynya."

Polynya formation in the open ocean has long been thought to have a thermodynamical origin associated with the upwelling of warm deep waters, a process brought on by static instability and vertical convection. The evidence presented here shows, on the contrary, that the fundamental mechanism explaining the Weddell Polynya is dynamical in origin. It is likely because of this surprising and perhaps counterintuitive dynamical origin that the mechanism of formation has eluded understanding for such a long time.

References and Notes

1. The word "polynya," of Russian origin, refers to an area of open water in sea ice and is distinguished from a lead.
2. P. Wadhams, *Ice in the Ocean* (Gordon and Breach Science, Amsteldijk, Netherlands, 2000), pp. 73–79.
3. M. G. McPhee *et al.*, *Bull. Am. Meteorol. Soc.* **77**, 1221 (1996).
4. R. D. Muench *et al.*, *J. Geophys. Res.* **106**, 2423 (2001).
5. C. L. Parkinson, W. M. Washington, *J. Geophys. Res.* **84**, 311 (1979).
6. R. Glowienka-Hense, *Beitr. Phys. Atmos.* **68**, 303 (1995).
7. R. Timmermann, P. Lemke, C. Kottmeier, *J. Phys. Oceanogr.* **29**, 1251 (1999).
8. D. G. Martinson, P. D. Killworth, A. L. Gordon, *J. Phys. Oceanogr.* **11**, 466 (1981).
9. T. Motoi, N. Ono, M. Wakatsuchi, *J. Phys. Oceanogr.* **17**, 2241 (1987).
10. H. W. Ou, *J. Phys. Oceanogr.* **21**, 1835 (1991).
11. K. Alverson, W. B. Owens, *J. Phys. Oceanogr.* **26**, 2196 (1996).
12. H. E. Huppert, K. Bryan, *Deep Sea Res.* **23**, 655 (1976).
13. D. R. Goldner, D. C. Chapman, *Deep Sea Res. Part I* **44**, 719 (1997).
14. A nondimensional parameter, the Rossby number $R_o = U_o/fL$, where U_o is the mean advective speed of the background flow (~10 cm/s), f is the Coriolis parameter (about -1.4×10^{-4} s^{-1}), and L is the width scale of the seamount (~100 km), can be used to characterize the flow regime. For $R_o \approx \vartheta(1)$, fluid goes up and over the seamount. For $R_o \approx 10^{-3}$, as is the case presently, fluid columns are compressed as they come aboard the seamount and acquire anticyclonic vorticity. As they debark the seamount, they stretch and acquire cyclonic vorticity.
15. V. V. Gouretski, A. I. Danilov, *Deep Sea Res. Part I* **40**, 561 (1993).
16. D. Olbers, V. Gouretzki, G. Seiss, J. Schroeter, *The Hydrographic Atlas of the Southern Ocean* (Alfred Wegener Institute, Bremerhaven, Germany, 1992) (available at www.awi-bremerhaven.de/Atlas/SO).
17. J. Verron, *Geophys. Astrophys. Fluid Dyn.* **35**, 257 (1986).
18. V. W. Ekman, *Arch. Math. Astron. Phys.* **2**, 1 (1905).
19. The horizontal frictional stress transmitted into the sea-ice cover from the action of the ocean currents is formulated as a quadratic drag law $\rho_o c_d |\vec{v}_o - \vec{v}_i|(\vec{v}_o - \vec{v}_i)$, where ρ_o is the seawater density, c_d is an empirical drag coefficient, and $\vec{v}_o$ and $\vec{v}_i$ are the ocean and sea-ice velocity fields, respectively. Under conditions of sea-ice divergence, the principal dynamical force balance is between this interfacial stress and the Coriolis force $fh_i\vec{v}_i$, a body force, where f is the Coriolis parameter and h_i is the sea-ice thickness. As a consequence of this force balance, sea ice in the Southern Hemisphere veers to the left of the ocean current vector. The degree of veering depends on the thickness of the sea ice and asymptotically approaches 90° for very thick sea ice. For the relatively thin floes in the vicinity of Maud Rise, the drift is ~20° to the left of the ocean current.
20. D. M. Holland, *Prog. Oceanogr.* **48**, 475 (2001).
21. R. Bleck, in *Ocean Modeling and Parameterization*, E. P. Chassignet, J. Verron, Eds. (Kluwer Academic, Dordrecht, Netherlands, 1998), pp. 423–448.
22. D. M. Holland, *J. Clim.* **14**, 1585 (2001).
23. *Data Announcement 88-MGG-02, Digital Relief of the Surface of the Earth* (NOAA, National Geophysical Data Center, Boulder, CO, 1988) (available at www.ngdc.noaa.gov/mgg/global/seltopo.html).
24. P. Gaspar, *J. Phys. Oceanogr.* **18**, 161 (1988).
25. Animations of the evolution of the sea-ice concentration, ocean surface flow, and ocean temperature fields are available at *Science* Online (www.sciencemag.org/cgi/content/full/292/5522/1697/DC1). Also included is supplementary text providing detail on the sea-ice–ocean model design.
26. F. D. Carsey, *Mon. Weather Rev.* **108**, 2032 (1980).
27. H. J. Zwally *et al.*, *Antarctic Sea Ice: 1973–1976: Satellite Passive-Microwave Observations*, *NASA SP-459* (NASA, Washington, DC, 1983).
28. M. R. Drinkwater, *ERS-1/2 Synthetic Aperture Data* (Jet Propulsion Laboratory, Pasadena, CA, 2001) (available at http://oceans-www.jpl.nasa.gov/mrd/Anzflux.html).
29. The Office of Polar Programs of the NSF supported this work through grants OPP-99-84966 and OPP-99-01039. Special thanks go to B. Lettau, without whose support this research would not have come into being.

25 January 2001; accepted 27 April 2001